J. Am. Soc. Mass Spectrom. (2016) 27:277–284
DOI: 10.1007/s13361-015-1275-y

RESEARCH ARTICLE

3D ToF-SIMS Analysis of Peptide Incorporation into MALDI Matrix Crystals with Sub-micrometer Resolution

Martin Körsgen,[1] Andreas Pelster,[1] Klaus Dreisewerd,[2,3] Heinrich F. Arlinghaus[1]

[1]Physikalisches Institut, University of Münster, 48149, Münster, Germany
[2]Institute for Hygiene, University of Münster, 48149, Münster, Germany
[3]Interdisciplinary Center for Clinical Research (IZKF), University of Münster, 48149, Münster, Germany

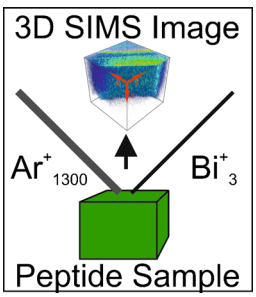

Abstract. The analytical sensitivity in matrix-assisted laser desorption/ionization mass spectrometry (MALDI-MS) is largely affected by the specific analyte-matrix interaction, in particular by the possible incorporation of the analytes into crystalline MALDI matrices. Here we used time-of-flight secondary ion mass spectrometry (ToF-SIMS) to visualize the incorporation of three peptides with different hydrophobicities, bradykinin, Substance P, and vasopressin, into two classic MALDI matrices, 2,5-dihydroxybenzoic acid (DHB) and α-cyano-4-hydroxycinnamic acid (HCCA). For depth profiling, an Ar cluster ion beam was used to gradually sputter through the matrix crystals without causing significant degradation of matrix or biomolecules. A pulsed Bi_3 ion cluster beam was used to image the lateral analyte distribution in the center of the sputter crater. Using this dual beam technique, the 3D distribution of the analytes and spatial segregation effects within the matrix crystals were imaged with sub-μm resolution. The technique could in the future enable matrix-enhanced (ME)-ToF-SIMS imaging of peptides in tissue slices at ultra-high resolution.
Keywords: ToF-SIMS, ME-SIMS, Ar cluster ion source, MALDI matrix, Analyte incorporation

Received: 31 March 2015/Revised: 4 September 2015/Accepted: 10 September 2015/Published Online: 29 September 2015

Introduction

Matrix-assisted laser desorption/ionization (MALDI) mass spectrometry is a powerful technique for the analysis of biomolecules [1]. The sensitivity of the method is determined by numerous factors, including in particular a "suitable" analyte-matrix interaction [2]. It is generally believed that an optimal detection limit for MALDI-MS of peptides and proteins is achieved if these are incorporated quantitatively in the matrix crystals [3, 4]. For other less polar compounds such as lipids [5] or polymers [6], these requirements are generally more relaxed, and thus a "loose contact" with the matrix is often sufficient for laser-induced co-desorption of both components (e.g., by deposition of analytes on top of a matrix surface or vice versa [7] or by mixing milled matrix and analyte [8]).

The incorporation of peptides and proteins into matrix crystals has, for example, been studied with confocal laser scanning microscopy (CLSM) [9–11] and field emission scanning electron microscopy (FE-SEM) [12]. These techniques provide high lateral resolution; however, they require the use of labeled proteins (e.g., for CLSM analytes have to be stained with dyes, and FE-SEM requires the use of Au cluster-labeled compounds). This bears the risk of altering the analyte incorporation and of producing artifacts (e.g., by detection of un-bound dyes or because of autofluorescence).

A label-free approach for studying analyte incorporation is the use of high resolution MS imaging. For example, Spengler and Hubert [13], and Bouschen and Spengler [14] used scanning microprobe MALDI-MS imaging to visualize the peptide distribution in surface areas of 2,5-dihydroxybenzoic acid (DHB) matrix crystals with a lateral resolution of ~1 μm, and Qiao et al. investigated–next to DHB preparations–two common cinnamic acid derivative matrices, α-cyano-4-hydroxy cinnamic acid (HCCA) and sinapic acid with a 10 μm-wide laser beam [15]. Both the Spengler and the Ens groups also explored the potential of their method for recording 3D profiles of the analyte distributions. Although this resulted in a coarse picture, finer details were difficult to obtain. The reasons lie in

Electronic supplementary material The online version of this article (doi:10.1007/s13361-015-1275-y) contains supplementary material, which is available to authorized users.

Correspondence to: Martin Körsgen; *e-mail:* martin.koersgen@uni–muenster.de

the non-uniform beam intensity profiles, causing a non-uniform ejection of material, as well as in the laser-induced degradation of the non-desorbed material. In particular for cinnamic acid-derived matrices, a strong deterioration of the ion signals is typically observed with an accumulating number of laser pulses applied to one position [16, 17]. This has been attributed to laser-induced thermal and photochemical modifications of the matrix compounds [18, 19]. Despite these limitations, the above MALDI-MS imaging studies clearly indicated the occurrence of analyte segregation within the analyte-matrix crystals; in particular the hydrophobicity of a compound seems to affect the overall co-crystallization process [14, 15]. Not least of such effects can have implications for MALDI-MS imaging and quantitative MALDI-MS analyses, because they can potentially affect the total ion signals obtained from a given pixel and within a given number of laser shots.

Time-of-flight secondary ionization mass spectrometry (ToF-SIMS) can image biological samples with nanometer-scale resolution [20] and is increasingly applied to numerous biological applications [21, 22]. The detection of biomolecules such as phospholipids (PL) and small peptides at these small focal sizes can be fostered by using bismuth cluster ion sources as well as by mixing the compounds into MALDI matrices for matrix-enhanced SIMS (ME-SIMS [23, 24]). For example, ME-SIMS has been used to record the distribution of PLs [25] as well as polymers [26] in the surface layers of DHB matrix preparations. Furthermore, ToF-SIMS was used to determine the lateral chemical displacement of biomolecules during the MALDI matrix preparation process [27]. However, whereas single-beam ToF-SIMS enables the analysis of a surface with high resolution, obtaining a depth profile of labile biomolecules within a sample is much more challenging because of the possible occurrence of radiation damages.

The use of an Ar gas cluster ion beam (GCIB) [28] provides a means for uniform sputtering of organic materials without causing extensive degradation of the underlying material [29]. Therefore, combining an Ar GCIB for sputtering with a Bi cluster ion beam for analysis (dual-beam ToF-SIMS) can potentially allow one to obtain high-resolution 3D images from organic materials. For example, the acquisition of 3D depth profiles of cholesterol as well as the detection of PLs in 14 µm thick rat brain slices has recently been demonstrated [30].

Here we used dual-beam ToF-SIMS to measure with sub-µm resolution the spatial distribution of bradykinin, Substance P, and vasopressin (representing three peptides with differing hydrophobicities) in DHB and HCCA MALDI crystals, prepared by the common dried-droplet method.

Experimental

Chemicals

All chemicals were purchased from Sigma-Aldrich (Schnelldorf, Germany) and used as supplied.

Sample Preparation

The peptides bradykinin (RFPSFGPPR-NH_2; MW: 1060.21 g/mol), Substance P (RPKPQQFFGLM-NH_2; MW: 1346.73 g/mol), and [Arg8]-vasopressin (CYFQNCPRG-NH_2; MW: 1083.45 g/mol; for simplicity in the following called vasopressin), were dissolved in distilled water to concentrations of 10^{-5} mol/L. DHB and HCCA were dissolved in distilled water/acetonitrile (1:1, v/v) to concentrations of 10^{-2} mol/L. Analyte and matrix solutions were first mixed to yield a molar analyte/matrix-ratio of 10^{-3} (for each peptide in a mixture); 2 µL (DHB) or 1.5 µL (HCCA) aliquots of the mixtures were then applied to a clean silicon wafer (used because of their flatness and conductibility). The crystallization took place at room temperature in a class 100 flow box. For obtaining reference mass spectra of neat peptides, 40 µL of pure peptide solutions were spin-coated onto a 1 × 1 cm^2 silicon wafer.

ToF-SIMS

The measurements were performed using a ToF-SIMS instrument that is widely compatible with the commercial ToF-SIMS V instrument (ION-TOF, Münster, Germany). Sputtering was performed with an Ar GCIB (ION-TOF) using 10 keV singly charged Ar ion clusters. A permanent magnet was used in the GCIB Wien filter system to obtain a narrow width of the Ar cluster distribution of 1300 ± 400 (FWHM). The average sputter current was about 3 nA. For analysis, a pulsed 30 kV liquid Bi ion source (LMIG, ION-TOF) with 0.5 nA direct current was employed. Bi_3 cluster ions were used as primary ions (PI) for analyzing and imaging the sample surface using the fast imaging mode of the LMIG with a pulse width of 100 ns. The Bi_3 beam was focused to ~100 nm diameter. Owing to the insulating properties and the surface topography of the samples, the actual lateral resolution of the 2D analysis was reduced to 400–500 nm, as was verified by measuring the edge sharpness of the analyzed crystals. The two ion cluster beams hit the sample from opposite directions at angles of incidence of 45° each. In order to increase the mass resolution m/Δm (FWHM) to >3000, delayed ion extraction was applied. All measurements were performed using the detection mode for positive secondary ions.

Data Acquisition and Image Generation

Mass spectra, MS images, and 3D reconstructions were obtained using SurfaceLab 6.4 software (ION-TOF). Lateral MS images were recorded with a pixel density of 256 × 256 by rastering the primary ion beam over an area of about 50 × 50 $µm^2$. To analyze the 3D molecular distributions of analyte and matrix species, the crystal was gradually sputtered off using the Ar GCIB. Typically, sputtering at a fluence of about $5*10^{14}$ PI/cm^2 was followed by ~100 s of analyses (10 scans). The time required to sputter through an entire matrix crystal could be identified both by the decrease of the matrix ion signals and by using a highly-resolving camera for sample observation mounted inside the ToF-SIMS instrument (see

below). To avoid shadowing effects, the area sputtered was larger by at least nine times than the area analyzed; the analysis area was located in the center of the sputter crater. Typically, several (up to five) identically prepared crystals were analyzed. Apart from some statistical variation, qualitatively consistent results were obtained. Representative results are presented within this paper.

Results and Discussion

Reference Mass Spectra

To identify characteristic signals of the peptides and the two matrices, reference mass spectra were recorded from neat samples under static SIMS conditions using the Bi_3 beam. The ToF-SIMS spectrum of spin-coated bradykinin (shown in Figure S-1a of the Electronic Supplementary Material) displays the molecular signal $[M + H]^+$ of bradykinin at *m/z* 1060.6, the signal of the doubly protonated molecule $[M + H_2]^{2+}$ at *m/z* 530.8, as well as numerous characteristic fragment ion signals. An intense fragment signal is found at *m/z* 70.1, presumably representing the $C_4H_8N^+$ immonium ion of the proline residue (calculated *m/z* 70.066). Because no sizable ion signal is found in the mass spectra of both matrices at this mass value (Figure S-2a, b), this last signal could, for the given sample, be used to sensitively identify bradykinin.

The two other peptides produce similar spectra containing the protonated molecular signal at *m/z* 1084.4 and *m/z* 1347.7 for vasopressin and Substance P, respectively (Figures S-1b, c). As for bradykinin, the most intense fragment ion can be found at *m/z* 70.1, which presumably is representing the proline-derived immonium ion ($C_4H_8N^+$).

The mass spectra recorded from neat matrix samples show strong signals of the molecular ions $[m + H]^+$ at *m/z* 155.0 (DHB; Figure S-2a) and *m/z* 190.0 (HCCA; Figure S-2b), respectively, and of the corresponding $[m - H_2O + H]^+$ fragments.

Determination of Sputter Rates

Optical images of typical DHB and HCCA crystals as obtained by the used dried-droplet sample preparation method are shown in Figure 1a, c. The DHB crystals exhibit a needle-like appearance with widths ranging from 20 to 70 µm and lengths up to 1000 µm, whereas more compact crystals are obtained for HCCA. Their sizes and shape varies to some extent with an average diameter of about 30 µm. The same morphologies were obtained from neat and from analyte-doped matrix crystals.

The sputter rate (i.e., the number of monolayers that are removed per given Ar PI fluence) can, in principle, be determined from the sputter time until a drop in signal intensity occurs after erosion of the crystal as is visible in Figure 1b, d, where parts of a ~1000 µm-wide DHB crystal and a full ~30 µm-wide HCCA crystal, respectively, were sputtered and the different signals were recorded as a function of sputter time. To determine the sputter rate, however, this requires precise knowledge of the height of the irradiated crystal. As shown schematically in Figure S-3, the initial height of a single irradiated crystal can be estimated from a series of ToF-SIMS images that are taken at different sputter times (proportional to removed crystal heights) and by recording the matrix ions. Images obtained at two different heights (assuming a rectangular parallelepiped crystal) exhibit a lateral offset of the crystal's side flank in the secondary ion image of the respective matrix signal $[m + H]^+$. At an angle of incidence of 45°, as used here, the offset is identical to the height of the sputtered structure (see Figure S-3). Using this approach, it was determined for DHB that a fluence of ~$0.7*10^{12}$ Ar cluster ions/cm^2 is necessary to remove 1 nm of the crystal. This value is in the same range as those previously obtained for other organic systems such as leucine films [31] and the organic semiconductor material NPD [32]. Owing to the stronger shaped structure (Figure 1d), the drop in signal intensity is less precipitous for the analyzed HCCA crystal and the sputter rates that are obtained using the same approach as above for DHB will be less precise. Assuming that most of the crystal is eroded after 800 s, a fluence of about $1.5*10^{12}$ Ar cluster ions/cm^2 is necessary to remove 1 nm of the HCCA crystal on average.

Bradykinin-Containing Matrix Crystals

To avoid possible interferences between the three test peptides and to ease the initial data interpretation, MALDI samples containing only the single peptide bradykinin were first analyzed.

Integral Depth Profiles

To analyze the incorporation of the peptide inside DHB and HCCA crystals, these were gradually sputtered off with the Ar GCIB beam. As above, a part of the elongated DHB and a full HCCA crystal were analyzed. Depth profiles are shown in Figure 1b, d. Each data point represents the sum signal intensity obtained by summation over the full 50 × 50 µm^2 and 40 × 40 µm^2 xy-cross sections, respectively, of the selected sputter area. The intensity of the molecular DHB signal $[m + H]^+$ is nearly constant over the full crystal depth (corresponding to a sputter time of ~160 s or 13.4 µm height; Figure 1b). Only the first data point, which represents the signal intensity obtained from the surface, obtained before the sputtering beam was turned on, shows a slightly lower intensity. Also, the molecular bradykinin signal $[M + H]^+$ and the bradykinin-derived immonium ion show a largely uniform distribution with depth z when the signal is averaged across the xy-plane. However, at the surface, elevated ion intensities (by a factor of about 5) are obtained. It is unlikely that the decrease of the bradykinin signal with successive sputtering is due to fragmentation caused by the Ar beam because the $C_4H_8N^+$ immonium ion signal

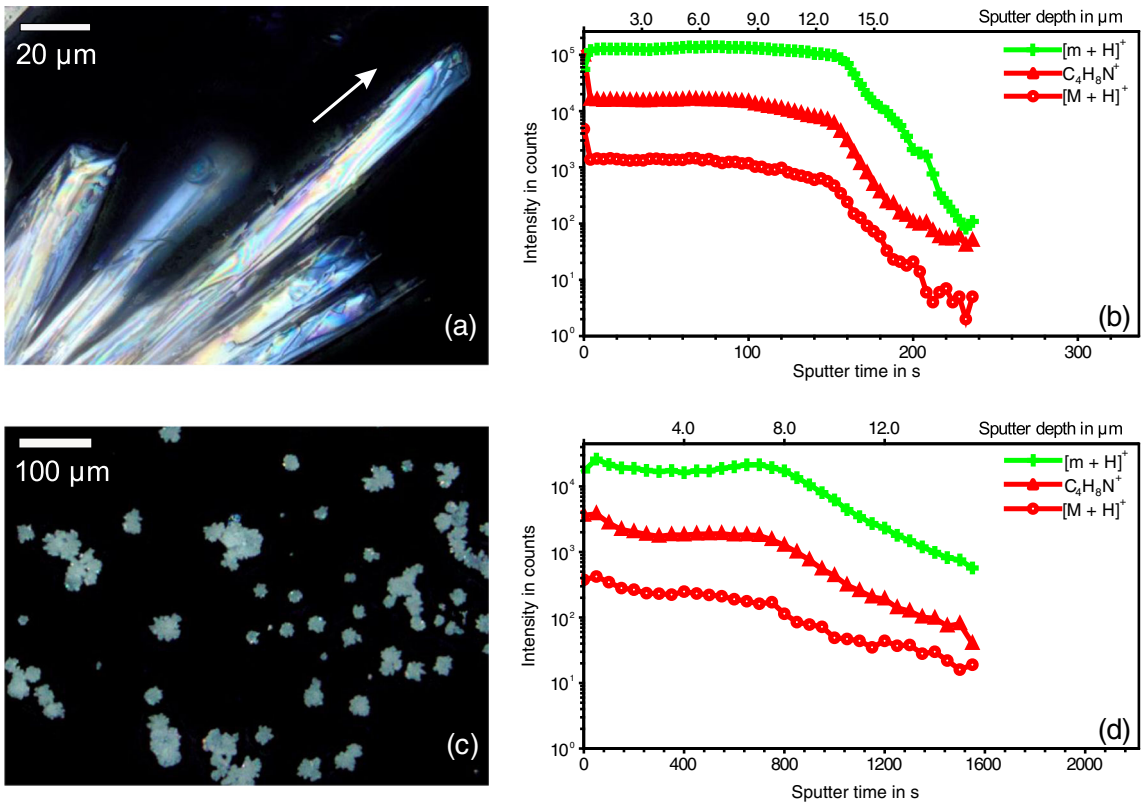

Figure 1. Optical images of (**a**) typical DHB, (**c**) HCCA crystals, and (**b**), (**d**) analyte and matrix ion signals as a function of sputter time (bottom axis) and estimated sputter depth (top axis; see text for further details); note the logarithmic intensity scale. The white arrow indicates the principal axis of the DHB crystal. The optical images were obtained using a polarization filter to gain a higher contrast with the surrounding silicon wafer

shows exactly the same dependence on sputter time as the protonated molecular signal. Thus, no significant fragmentation by the Ar cluster beam is observable and undisturbed 3D depth profiles of the intact molecular biomolecules can be obtained with high depth resolution. Therefore, the increased peptide signals that are obtained at the crystal surface indicate an enrichment of the analyte in the surface region. Similar results were indicated in previous MALDI-MS studies with the DHB matrix [17].

Sputter profiles of the matrix and peptide ions recorded from a typical HCCA crystal are depicted in Figure 1d. In comparison to the measurements of the bradykinin-doped DHB samples, lower matrix and analyte ion signals are obtained, probably because of a lower ionization efficiency of the HCCA matrix. In contrast to DHB, both matrix- and peptide-derived ion signals show a slight dip at the surface and a shallow local maximum in ion production at a depth of about 0.7 µm. Again, the molecular bradykinin and the immonium ion show exactly the same trend. A very minor decline of both signals (within a factor of 2–3) with increasing sputter time is probably caused by the changes in the matrix diameter, or possibly some spatial segregation effect, rather than by an Ar beam-induced degradation of matrix or analytes. This differentiates the method from the MALDI analysis of cinnamic acid derivatives, where laser-induced thermal-/photochemical modifications degrade the matrix performance [15–19].

Lateral Analyte Distribution at Different Crystal Depths

Figure 2 shows the 2D distribution of bradykinin across the initial top crystal surface and at approximately 1/3 depth. It should be noted that this depth can only be an estimation because the flank facing the sputter gun is sputtered simultaneously at different heights because of the grazing irradiation of the sputter beam. For the DHB crystal, an enrichment of the peptide is observed in the side flanks of the matrix crystal whereas a partial depletion in the central area is notable at both crystal heights. Interestingly, also the matrix ion signals show some variation with position, which could reflect irregular crystal morphologies or other crystal defects [12]. Line scans across the crystals (as depicted by the white rectangles in Figure 2) reveal that the bradykinin signal intensity varies by a factor of ~4 across the DHB crystal cross section and that the surface area with higher bradykinin intensities is about 6 to 8 µm wide (Figure 2c, f); the summation over a 2 µm-wide cutaway used to evaluate the line scan data was necessary to reduce the fluctuations produced by the low intensity of a single line scan. The constancy of the matrix ion signal in the central area of the crystal as well as the essentially constant ratio between molecular peptide ion and immonium fragment (not shown) indicate that a constant ionization efficiency is obtained. Thus, the measured intensities of the analyte signals

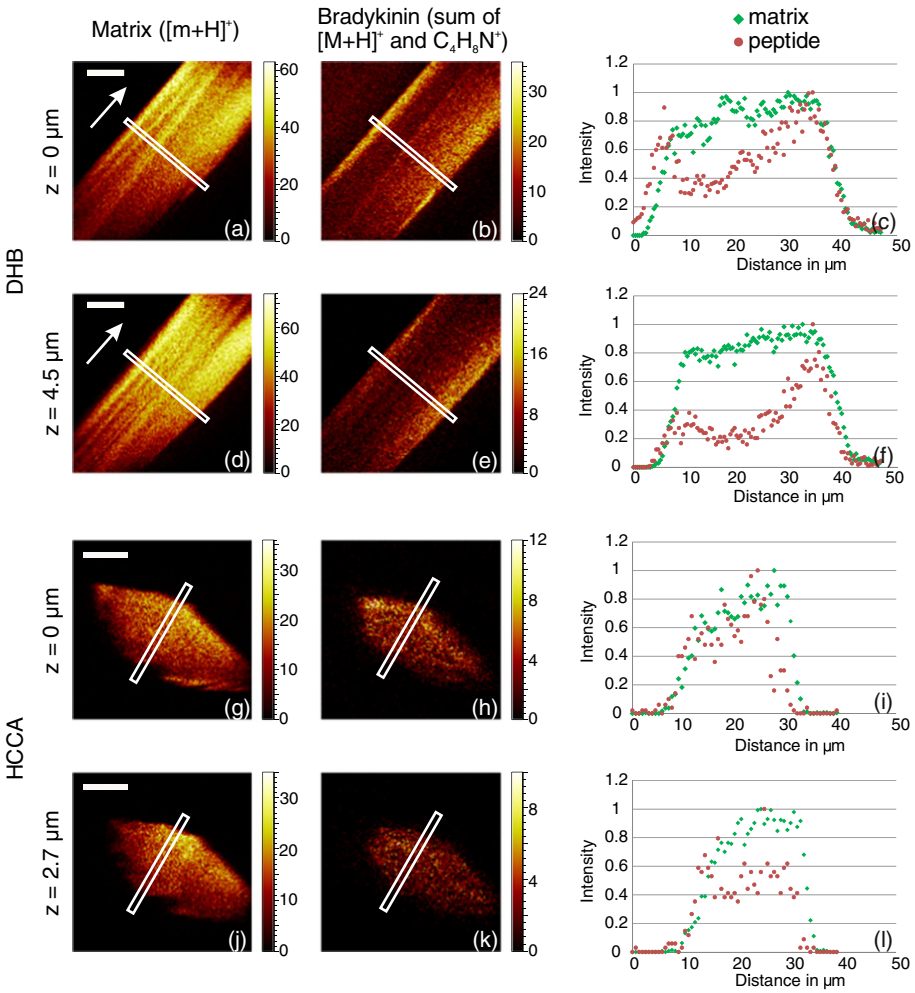

Figure 2. Left and middle: 2D distribution of bradykinin- and matrix-derived ions obtained across the initial top surface of a DHB and a HCCA crystal and after sputtering about one-third of the crystals. Scale bar: 10 µm. The white arrows indicate the principal axis of the DHB crystal. The color scale indicates the measured intensity in counts. Right: line scans of the normalized (maximum intensity) matrix and peptide signals across the crystals; the approximate scanned area is depicted by the white rectangles

should correlate with the concentration of the embedded analyte. Also, for the HCCA matrix, some variation in the incorporation of the bradykinin is notable in the line scans (Figure 2i, l), though to a much smaller extent than for DHB. In tendency, slight peptide enrichment is here notable towards the center of the crystal. The "depletion zone" at the side surfaces is approximately 3 µm wide.

3D-Distribution

Figure 3a, b depict the reconstructed spatial distribution of bradykinin within the investigated DHB crystal shown in Figure 2. To increase the signal contrast, the immonium fragment ion was evaluated in this case because of its higher signal intensity compared with the molecular ion. Moreover, binning of 4 pixels for the x-y plane and 2 pixels for the z-axis was employed, resulting in a voxel size of approximately 0.4 × 0.4 × 0.5 µm^3 (xyz). Also, the 3D image shows that the highest ion signals are obtained from the top surface and that some further enrichment occurs in the side flanks of the DHB crystal. The latter is best seen in the cross section through the crystal, performed at 50% of the y-axis value (Figure 3b), as well as in a video animation of the crystal available as Electronic Supplementary Material.

During the first scan of the Bi_3^+ beam (before any sputtering with the Ar GCIB), low-intensity signals of the bradykinin-derived immonium fragment are also detected next to the DHB crystal (i.e., directly from the Si wafer surface). Note that due to the conversion from sputter time into depth, the z-position of the silicon wafer is in this case not reflected correctly (i.e., these ion signals are represented as if originating from the top plane of the DHB crystal [z = 13.5 µm]). Presumably, these ions are representing analyte molecules that have not co-crystallized with the matrix within the dried-droplet sample preparation step, and thus formed a thin layer on the silicon wafer. In contrast, DHB-

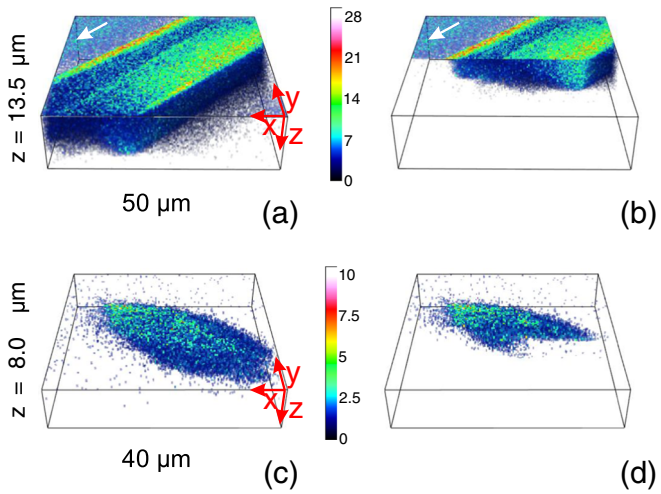

Figure 3. Reconstructed 3D distribution of bradykinin (evaluated from the fragment signal $C_4H_8N^+$) in (**a**) DHB and (**c**) HCCA crystals. (**b**), (**d**) Cutaways at 50% of the crystal width. Scanned areas were 50 × 50 µm^2 (DHB) and 40 × 40 µm^2 (HCCA) wide. The white arrows indicate the principal axis of the DHB crystal. The color scale indicates the measured intensity in counts

derived ions are not detected in notable abundance in these areas. After the first scan of the Ar sputter ion beam, these ion signals are essentially eliminated (see Figure 3b). However, a second group of low abundance bradykinin-derived "off-crystal ions" is detected after additional Ar ion beam scans. These can be explained by deposition of sputtered material on the wafer surface with consecutive analysis. Because the Ar sputter beam is hitting the target from the left side in Figure 3, crystal material seems to be mainly deposited to the opposite (right) side. This assumption is corroborated by the detection of low-intensity matrix ion signals in these areas (not shown).

As was already indicated by the data of Figures 1 and 2, for the investigated HCCA crystal, peptide enrichment is visible in the upper parts of the volume and in tendency in the central part of the crystal (Figure 3c, d). In contrast to the DHB sample, less bradykinin signals are found on the Si wafer around the crystal, suggesting that a more complete co-crystallization might have occurred in this case. Please see the Electronic Supplementary Material for a video animation of the HCCA crystal.

Segregation Effects

A typical measure for the hydrophobicity of an analyte is the so-called Bull and Breeze (B&B) index [33], which essentially uses the surface tension of dissolved amino acids (or combinations thereof as in the case of the peptides) between the water–air interface to calculate their hydrophobicity. The three test peptides vasopressin, bradykinin, and Substance P exhibit B&B indices of 960, −940, and −1790, respectively and, therefore, span the range of a more hydrophilic (vasopressin) to increasingly more hydrophobic peptides (bradykinin and substance P).

2D cross-section images reflecting the incorporation of the three peptides in the two matrix crystals with the initial surface elements (z = 0) and at depths of 2.1 (DHB) and 2.8 µm (HCCA), representing sections of the half crystals, respectively, are depicted in Figure 4 (left). Note that in comparison to the DHB crystal analyzed above, this one exhibits a lower thickness of 4.2 µm. Scans, representing the overall distribution of the three analytes as a function of depth z (integrated over the xy-cross section), are presented in the right part of the figure.

Upon preparation from the peptide mixture, bradykinin is distributed notably differently throughout the DHB crystal than if prepared as a single compound. By far the highest signal intensities are now obtained toward the left flank of the matrix crystal and in the top surface region. In contrast, there is little effect of the position with regard to the main axis of the needle-like DHB crystal (indicated by a white arrow). A similar pronounced spatial segregation effect is notable for Substance P. A comparison between the three distributions is depicted in the overlay image (utmost right column in Figure 4a, b), were the molecular ions of bradykinin are represented in green, those of vasopressin in blue, and those of Substance P in red. The overlay indicates that Substance P is located more to the left flank than bradykinin. This indicates that the separation is driven by the hydrophobicity, i.e., the peptide with the highest negative B&B index (Substance P) shows the largest separation followed by the peptide with the second highest one (bradykinin). Vasopressin (representing the most polar compound) is incorporated much more homogenously. The depth profile of this compound, depicted in Figure 4c, shows a strong decrease of the bradykinin signal (green) in comparison to the vasopressin signal (blue), indicating that bradykinin is more incorporated in the upper part of the crystal, whereas vasopressin is almost uniformly distributed throughout the crystal. These data suggest that the DHB crystal may have grown from bottom to top and right to left and that the hydrophilic vasopressin was preferentially incorporated first. Generally, the hydrophobicity of analyte and matrix, the solvent composition, the mass of the analyte, and the speed of the crystallization will all influence fine details of the incorporation [15]. The

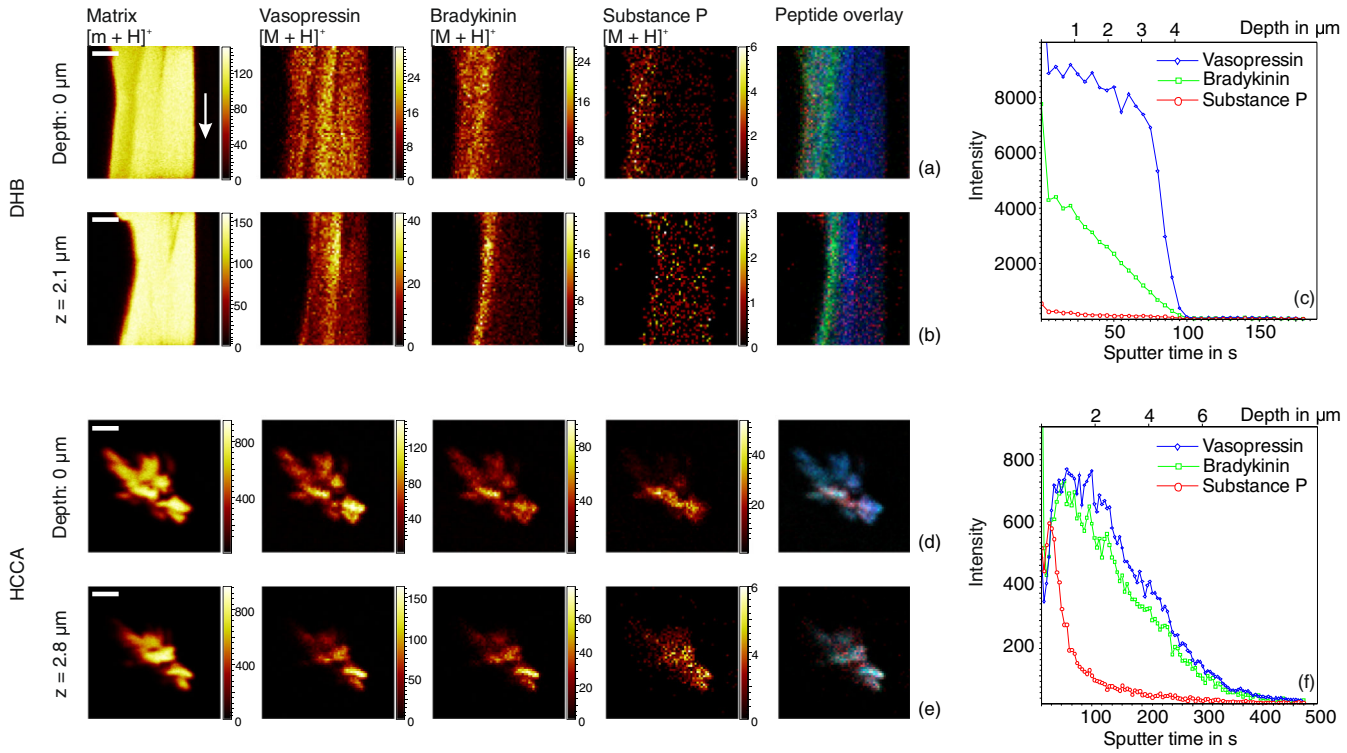

Figure 4. **Left**: Lateral distribution of the $[M + H]^+$ signals of vasopressin, bradykinin, and Substance P, and matrix-derived signals $[m + H]^+$. Data were recorded at the initial top surface and after sputtering part of the crystal. Scanned areas were 50 × 50 µm² wide; scale bar: 10 µm. The color scale indicates the measured intensity in counts. **Right**: $[M + H]^+$ ion signals of the investigated peptides as a function of sputter time (the approximated sputter depth is denoted at the top axis)

observation of these segregation effects between peptides with different hydrophobicities in a DHB crystal is in agreement with the previous MALDI-MSI studies that incorporated the same or similar analytes into the matrices [14, 15]. However, due to the removal of monolayers of material without accumulating a significant amount of molecular damage, this is the first study enabling a 3D analysis at high resolution.

For the HCCA crystals, a stronger segregation effect is only visible for the more hydrophobic Substance P, which is mainly incorporated in the crystals surface (Figure 4f). The difference to DHB could be due to the faster crystallization of the smaller crystals.

Conclusion

Dual ion beam ToF-SIMS is a powerful tool for determining the spatial distribution of peptides with masses in the 1 kDa range within an organic matrix such as a MALDI matrix crystal. The demonstrated sub-µm resolution sets a benchmark figure and, together with the soft sputtering achieved by the Ar GCIB, allows revealing fine features of the analyte-matrix co-crystallization, for example with regard to the visualized surface enrichment effects and hydrophobicity-driven segregation effects. The method could be helpful for developing improved MALDI sample preparation protocols. Moreover, the achieved sub-µm-resolution makes the ME-SIMS approach extremely interesting for high resolution MS imaging of peptide distributions in tissue slices.

Acknowledgments

The authors thank Jamie Yeoh of Keyence Microscope Europe for measuring crystal heights with their laser scanning microscope and Volker Vehof and Jens Soltwisch for technical support and helpful discussions. Financial support by the German Science Foundation (grant DR 416/9-1) and the IZKF Münster (grant Z03) is gratefully acknowledged.

References

1. Hillenkamp, F., Peter-Katalinić, J. (eds.): MALDI MS—A Practical Guide to Instrumentation, Methods, and Applications, 2nd edn. Wiley-Blackwell, Weinheim (2013)
2. Dreisewerd, K.: The desorption process in MALDI. Chem. Rev. **103**, 395–425 (2003)
3. Glückmann, M., Pfenninger, A., Krüger, R., Thierolf, M., Karas, M., Horneffer, V., Hillenkamp, F., Strupat, K.: Mechanisms in MALDI analysis: surface interaction or incorporation of analytes? Int. J. Mass Spectrom. **210/211**, 121–132 (2001)
4. Horneffer, V., Glückmann, M., Krüger, R., Karas, M., Strupat, K., Hillenkamp, F.: Matrix-analyte-interaction in MALDI-MS: pellet and nano-electrospray preparations. Int. J. Mass Spectrom. **249/250**, 426–432 (2006)
5. Marto, J.A., White, F.M., Seldomridge, S., Marshall, A.G.: Structural characterization of phospholipids by matrix-assisted laser desorption/ionization Fourier transform ion cyclotron resonance mass spectrometry. Anal. Chem. **67**, 3979–3984 (1995)

6. Nielen, M.W.F.: MALDI time-of-flight mass spectrometry of synthetic polymers. Mass Spectrom. Rev. **18**, 309–344 (1999)
7. Hankin, J.A., Barkley, R.M., Murphy, R.C.: Sublimation as a method of matrix application for mass spectrometric imaging. J. Am. Soc. Mass Spectrom. **18**, 1646–1652 (2007)
8. Skelton, R., Dubois, F., Zenobi, R.: A MALDI sample preparation method suitable for insoluble polymers. Anal. Chem. **72**, 1707–1710 (2000)
9. Dai, Y., Whittal, R.M., Li, L.: Two-layer sample preparation: a method for MALDI-MS analysis of complex peptide and protein mixtures. Anal. Chem. **68**, 2494–2500 (1996)
10. Strupat, K., Karas, M., Hillenkamp, F.: 2,5-Dihydroxybenzoic acid: a new matrix for laser desorption-ionization mass spectrometry. Int. J. Mass Spectrom. Ion Process **111**, 89–102 (1991)
11. Horneffer, V., Forsmann, A., Strupat, K., Hillenkamp, F., Kubitscheck, U.: Localization of analyte molecules in MALDI preparations by confocal laser scanning microscopy. Anal. Chem. **73**, 1016–1022 (2001)
12. Horneffer, V., Reichelt, R., Strupat, K.: Protein incorporation into MALDI-matrix crystals investigated by high resolution field emission scanning electron microscopy. Int. J. Mass Spectrom. **226**, 117–131 (2003)
13. Spengler, B., Hubert, M.: Scanning microprobe matrix-assisted laser desorption ionization (SMALDI) mass spectrometry: instrumentation for sub-micrometer resolved LDI and MALDI surface analysis. J. Am. Soc. Mass Spectrom. **13**, 735–748 (2002)
14. Bouschen, W., Spengler, B.: Artifacts of MALDI sample preparation investigated by high-resolution scanning microprobe matrix-assisted laser desorption/ionization (SMALDI) imaging mass spectrometry. Int. J. Mass Spectrom. **266**, 129–137 (2007)
15. Qiao, H., Piyadasa, G., Spicer, V., Ens, W.: Analyte distributions in MALDI samples using MALDI imaging mass spectrometry. Int. J. Mass Spectrom. **281**, 41–51 (2009)
16. Fournier, I., Beavis, R.C., Blais, J.C., Tabet, J.C., Bolbach, G.: Hysteresis effects observed in MALDI using oriented, protein-doped matrix crystals. Int. J. Mass Spectrom. **169/170**, 19–29 (1997)
17. Wiegelmann, M., Soltwisch, J., Jaskolla, T.W., Dreisewerd, K.: Matching the laser wavelength to the absorption properties of matrices increases the ion yield in UV-MALDI mass spectrometry. Anal. Bioanal. Chem. **405**, 6925–6932 (2013)
18. Tarzi, O., Nonami, H., Balsells, R.E.: The effect of temperature on the stability of compounds used as UV-MALDI-MS matrix: 2,5-dihydroxybenzoic acid, 2,4,6-trihydroxyacetophenone, α-cyano-4-hydroxycinnamic acid, 3,5-dimethoxy-4-hydroxycinnamic acid, norharmane, and harmane. J. Mass Spectrom. **44**, 260–277 (2009)
19. Hoyer, T., Tuszynski, W., Lienau, C.: Ultrafast photodimerization dynamics in α-cyano-4-hydroxycinnamic and sinapinic acid crystals. Chem. Phys. Lett. **443**, 107–112 (2007)
20. Draude, F., Körsgen, M., Pelster, A., Schwerdtle, T., Müthing, J., Arlinghaus, H.F.: Characterization of freeze-fractured epithelial plasma membranes on nanometer scale with ToF-SIMS. Anal. Bioanal. Chem. **407**, 2203–2211 (2015)
21. Proceedings of the 18th International Conference on Secondary Ion Mass Spectrometry, SIMS XVIII. Riva Del Garda, Trento, Italy, September 18–23, Surf. Interface Anal. **45**, (2011)
22. Proceedings of the 19th International Conference on Secondary Ion Mass Spectrometry, SIMS XIX. Jeju, Korea, September 29–October 4, Surf. Interface Anal. **46**, (2013)
23. Wu, K.J., Odom, R.W.: Matrix-enhanced secondary ion mass spectrometry: a method for molecular analysis of solid surfaces. Anal. Chem. **68**, 873–882 (1996)
24. Delcorte, A.: Matrix-enhanced secondary ion mass spectrometry: the Alchemist's solution? Appl. Surf. Sci. **252**, 6582–6587 (2006)
25. Luxembourg, S.L., McDonnell, L.A., Duursma, M.C., Guo, X., Heeren, R.M.A.: Effect of local matrix crystal variations in matrix-assisted ionization techniques for mass spectrometry. Anal. Chem. **75**, 2333–2341 (2003)
26. Hanton, S.D., Clark, P.A.C., Owens, K.G.: Investigations of matrix-assisted laser desorption/ionization sample preparation by time-of-flight secondary ion mass spectrometry. J. Am. Soc. Mass Spectrom. **10**, 104–111 (1998)
27. Passarelli, M.K., Wang, J., Mohammadi, A.S., Trouillon, R., Gilmore, I., Ewing, A.G.: Development of an organic lateral resolution test device for imaging mass spectrometry. Anal. Chem. **86**, 9473–9480 (2014)
28. Yamada, I., Matsuo, J., Toyoda, N., Kirkpatrick, A.: Materials processing by gas cluster ion beams. Mater. Sci. Eng. R Rep. **34**, 231–295 (2001)
29. Niehuis, E., Möllers, R., Rading, D., Brüner, P.: Dual beam depth profiling of organic materials: assessment of capabilities and limitations. Surf. Interface Anal. **46**, 70–73 (2014)
30. Bich, C., Havelund, R., Möllers, R., Touboul, D., Kollmer, F., Niehuis, E., Gilmore, I.S., Brunelle, A.: Argon cluster ion source evaluation on lipid standards and rat brain tissue samples. Anal. Chem. **85**, 7745–7752 (2013)
31. Ichiki, K., Ninomiya, S., Nakata, Y., Honda, Y., Seki, T., Aoki, T., Matsuo, J.: High sputtering yields of organic compounds by large gas cluster ions. Appl. Surf. Sci. **255**, 1148–1150 (2008)
32. Ninomiya, S., Ichiki, K., Yamada, H., Nakata, Y., Seki, T., Aoki, T., Matsuo, J.: Molecular depth profiling of multilayer structures of organic semiconductor materials by secondary ion mass spectrometry with large argon cluster ion beams. Rapid Commun. Mass Spectrom. **23**, 3264–3268 (2009)
33. Bull, H.B., Breese, K.: Surface tension of amino acid solutions: a hydrophobicity scale of the amino acid residues. Arch. Biochem. Biophys. **161**, 665–670 (1974)